Reynolds Force Evaluation of Quasi-Coherent Structure by Tomographic Laser-Induced Fluorescence Spectroscopy

Hiroyuki ARAKAWA, Makoto SASAKI[1)], Shigeru INAGAKI[2,3)] and Akihide FUJISAWA[3,4)]

Department of Health Sciences, Faculty of Medical Sciences, Kyushu University, Fukuoka 812-8582, Japan
[1)]*College of Industrial Technology, Nihon University, Narashino 275-8575, Japan*
[2)]*Institute of Advanced Energy, Kyoto University, Uji 611-0011, Japan*
[3)]*Research Centre for Plasma Turbulence, Kyushu University, Kasuga 816-8580, Japan*
[4)]*Research Institute for Applied Mechanics, Kyushu University, Kasuga 816-8580, Japan*

(Received 20 December 2022 / Accepted 27 March 2023)

A new method of vector tomography by laser-induced fluorescence (LIF) spectroscopy is proposed for the evaluation of the velocity field of quasi-coherent structure in linear magnetized plasma. Here, the two-dimensional velocity field was reconstructed with measuring synchronization of azimuthal reference probes and line-integrated LIF. The laser installation condition is designed to move in a radial direction perpendicular to the laser path. We applied the proposed method to a quasi-coherent flow obtained from a direct numerical turbulence simulation and demonstrated that the Reynolds stress and its force can be evaluated if its flow structure is maintained.

Keywords: magnetized plasma, laser-induced fluorescence, vector tomography, two-dimensional velocity field, Reynolds force

DOI: 10.1585/pfr.18.1401032

1. Introduction

In magnetized plasma, it has been known that turbulence induces coherent flows, *e.g.*, streamer [1], solitary eddy [2, 3] and zonal flow [4]. Interactions between the coherent flows and turbulence significantly affect plasma transport [4]. Thus, there is a need for two- or three-dimensional velocity field measurement since the coherent flows have a multi-scale structure, *i.e.*, the zonal flow has azimuthally elongated and radially localized structure. The multiple-Langmuir probe has been actively used in the measurement of the dynamic interactions of multi-scale couplings between the flows and the turbulence [1–3, 5–7]. However, the Langmuir probe perturbs the plasma around the central plasma region, because of which it is difficult to measure the flows and the turbulence around the center. Hence, new measurement techniques for identifying the velocity field are required to further understand the fundamental interaction of turbulence and flows.

In this regard, the tomographic method can be considered a suitable method for detecting multi-scale flow structure. This method can reconstruct the local information using integrated values, *e.g.*, line-integration of light emission intensity of the plasma [8]. Especially, vector tomography, which can reconstruct the velocity field, has been actively being developed [9–13]. However, tomographic methods require the multiple-projection angles to reconstruct the local structure. Given their physical limitation of projection angle, most of these developed methods can allow only cylindrical symmetry and/or have low spatial resolution that make it difficult for them to evaluate the multi-scale interaction of turbulence.

In this study, we propose a new method of tomographic laser-induced fluorescence spectroscopy (LIF) for measuring the velocity field of quasi-coherent flow in a linear magnetized plasma. For this, it is ensured that the flow propagates azimuthally while maintaining its structure. The sinogram, projection profiles with multiple-projection angle, is reconstructed by synchronizing the line-integrated LIF with the measurements of the azimuthal Langmuir probe array. Feasibility tests are carried out using the data of numerical turbulence simulation, as described in previous studies [14, 15]. Our evaluations included the data of ideally coherent flow structure and quasi-coherent flow structure. For simulation of the measurement, conditions similar to practical measurement conditions, such as the practical intervals of laser injection positions (~ 2 mm), laser frequency shift intervals (0.1 GHz), and projection angle intervals ($2\pi/64$ rad) were applied. The Reynolds stress and its force were also evaluated in this study.

2. Method

2.1 Target discharge

Magnetized plasma in linear devices, such as the LMD-U [1, 2] and PANTA [7, 8], were considered. These plasmas have a simple cylindrical shape, and the magnetic field has an axial direction with uniform intensity. These devices are dedicated to the fundamental process

author's e-mail: arakawa.hiroyuki.306@m.kyushu-u.ac.jp

of plasma turbulence and generate cylindrical magnetized plasma with a diameter of ~10 cm and a length of ~4 m. The typical plasma parameters on Argon plasma at the central region is ~1× 10^{19} m^{-3} electron density (n_e), ~3 eV electron temperature (T_e) and ~0.3 eV ion temperature (T_i) at the condition of 3 kW RF power, 2 mTorr neutral gas pressure and 0.09 T magnetic field strength. The turbulence state can be selected by magnetic field strength, filling neutral gas pressure and the heating power [5]. In this study, the target plasma is rotating at a coherent structure quasi-periodically, as observed in Ref. [2, 3].

2.2 Basics and measurement system

The LIF is a spectroscopy diagnostic method that measures the Doppler resolved ion velocity distribution functions (IVDF) [16, 17] using the fluorescence intensity at level transition of ions. The IVDF depends on ion density, ion temperature, ion velocity, and direction of laser injection line.

A schematic view of the proposed measurement system by tomographic LIF is shown in Fig. 1 (a). The proposed system consists of (i) a narrow-band laser with frequency scanning system, (ii) a movable stage for changing the injection position of the laser relative to the plasma center, (iii) an azimuthal probe array with measuring ion saturation current or floating potential for identifying the propagation of the quasi-coherent structure, and (iv) optics for collecting line-integrated fluorescence. Other devices for measuring the fluorescence intensity, such as a photo multiplier tube and a lock-in-amplifier system with high-frequency laser switch, are also required for the measurements.

Figures 1 (b), (c) and (d) illustrate the definition of the variables and the coordinates. The stationary and rotating coordinate systems are perpendicular to the magnetic field and are centered at the plasma axis. A position in the stationary coordinate system is shown as $\boldsymbol{r} = (x, y)$. The relationship to the azimuthal probe array in the plane is shown in Fig. 1 (b). Here, the azimuthal probe array is considered to be installed the one in PANTA [1]. The Langmuir probes in the azimuthal probe array were aligned in the azimuthal direction (θ) with equal spacing along a circle with a radius r_p. The θ_j ($j = 1, 2, 3, \cdots, N$) in the figure indicates the azimuthal position of each probe in the stationary coordinate system when the circle is divided into N segments. The azimuthal phase of the rotating quasi-coherent structure was set to ϕ. Figure 1 (c) shows the case when the structure has an initial phase $\phi = 0$, and Fig. 1 (d) shows the case when the structure rotates ϕ. A position in the rotating coordinate system is defined as

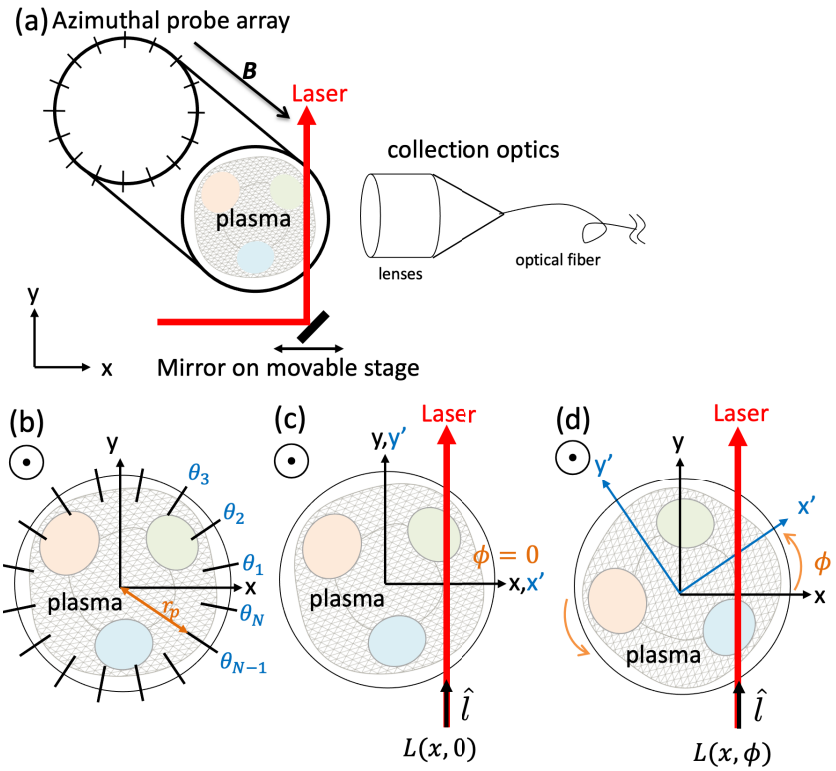

Fig. 1 (a) Schematic view of the reference probe (azimuthal probe array), the laser irradiation setup and collecting optics. (b) Alignment of the the azimuthal probe array with an azimuthal spacing of $2\pi/N$ rad on the stationary coordinate system. (c) and (d) Illustration of laser incidence conditions and changes in the situation for different ϕ. The ϕ indicates the azimuthal rotation phase of the structure. The $L(x,\phi)$ indicates the laser path in the structure with respect to the laser incidence position (x) and ϕ. The $\hat{\boldsymbol{l}}$ denotes the unit vector of L.

$\boldsymbol{r}' = (x', y') = (x\cos\phi + y\sin\phi, -x\sin\phi + y\cos\phi)$. The laser was injected at a position x parallel to the y axis and a laser frequency ν. The laser path in the rotating structure corresponds to $L(x, \phi)$ and the unit vector of L is $\hat{\boldsymbol{l}}(\phi)$. Under the conditions of Figs. 1 (c) or (d), they are denoted as $L(x,0)$ or $L(x,\phi)$, respectively.

The local fluorescence $\epsilon(\nu; \boldsymbol{r}', \hat{l})$ at position $\boldsymbol{r}' = (x', y')$ can be shown as Gaussian line profile as previously discussed [9, 12]:

$$\epsilon(\nu; \boldsymbol{r}', \hat{l}) = \frac{\epsilon_0(\boldsymbol{r}')}{\sqrt{2}\sigma(\boldsymbol{r}')} \exp[-(\nu' - u(\boldsymbol{r}'))^2/(2\sigma^2(\boldsymbol{r}'))], \tag{1}$$

where $\epsilon_0(\boldsymbol{r}')$ denotes the spectral integration of local fluorescence intensity, $\sigma(\boldsymbol{r}')$ denotes the line broadening caused by ion temperature (T_i) and the mass of ions (m_i) as $\sigma^2(\boldsymbol{r}') = kT_i(\boldsymbol{r}')/m_ic^2$, c denotes the speed of light, $\nu' = (\nu - \nu_0)/\nu_0$ denotes a normalized frequency, ν_0 denotes the fluorescence line center, $u(\boldsymbol{r}') = \boldsymbol{u}(\boldsymbol{r}') \cdot \hat{l} = \boldsymbol{v}(\boldsymbol{r}')/c \cdot \hat{l}$ denotes the normalized Doppler frequency shift, $\boldsymbol{u}(\boldsymbol{r}')$ denotes the normalized velocity field and $\boldsymbol{v}(\boldsymbol{r}')$ denotes the velocity field. The local fluorescence depends on the direction of laser injection angle ($\hat{l}$) relative to azimuthal phases of the rotating structure. Thus, the multiple laser path relative to the rotation structure, $L(x, \phi)$, should be identified to determine the local flow vector.

The line-integration of fluorescence along the line $L(x, \phi)$ is given as,

$$I(\nu'; x, \phi) = \int_{L(x,\phi)} \epsilon(\nu'; \boldsymbol{r}', \hat{l}) dl. \tag{2}$$

While maintaining the flow structure, the laser position (x) was changed to cover the whole plasma region by moving the movable stage parallel to the x-axis, and the laser frequency (ν') was scanned around the stable state of ions.

In correspondence with the experiment, the line-integrated fluorescence intensity is measured as $I(t)$ in time and the azimuthal probe array data is simultaneously measured its azimuthally-temporal structure as $f(\theta, t)$ during plasma discharge. This method is designed to obtain $I(\nu'; x, \phi)$ from $I(t)$ by conditional averaging using laser incidence conditions and an azimuthal probe array data. The procedure for this analysis method and the reconstruction of the velocity field are described in the next subsection.

2.3 Analytic procedure

The reconstruction method of vector tomography for spectroscopic measurement was proposed such as in [9, 12]. Note that this reconstruction method is applicable in the case of divergence-free flow [18]. Here, we briefly summarize the analytic procedure for applying our measurement system.

Measurement of azimuthal probe array identified the azimuthal phases of the quasi-periodic structure (ϕ). The ϕ is analyzed as,

$$\phi(t) = \frac{1}{m_p} \int_{t_0}^{t} \left[\frac{d}{dt'} \left(\arctan \frac{\Im[F(m_p, t')]}{\Re[F(m_p, t')]} \right) \mod 2\pi \,\text{rad} \right] dt', \tag{3}$$

where the $F(m_p, t)$ indicates the instantaneous azimuthal Fourier transform with azimuthal probe array data $f(\theta, t)$ [6], $\Re$ or $\Im$ denotes the the real or imaginary part of the Fourier transform, t_0 denotes the reference time, and m_p denotes the reference azimuthal mode number, which is related to the wave number (k_θ) as $m_p = 2\pi r_p k_\theta$. The time variation of the fluorescence intensity $I(t)$ was then converted by conditional averaging to $I(\nu'; x, \phi)$ by knowing the time dependence of ϕ and by the conditions of the laser incident position (x) and frequency (ν').

The spectral moment is introduced to reconstruct the local velocity distribution and is defined as [9],

$$\mu^{(n)} = \int_{-\infty}^{\infty} I(\nu'; x, \phi) \nu'^n d\nu', \tag{4}$$

where n denotes the order of spectral moment. The spectral moment of 0^{th} and 1^{st} order can be shown by using $\epsilon_0(\boldsymbol{r}')$ and $\boldsymbol{u}(\boldsymbol{r}')$ as [9],

$$\mu^{(0)}(x, \phi) = \int_{L(x,\phi)} \epsilon_0(\boldsymbol{r}') dl \tag{5}$$

and

$$\mu^{(1)}(x, \phi) = \int_{L(x,\phi)} \epsilon_0(\boldsymbol{r}') \boldsymbol{u}(\boldsymbol{r}') \cdot d\hat{l}. \tag{6}$$

Equation (5) is a sinogram of scalar tomography for $\epsilon_0(\boldsymbol{r}')$. Equation (6) is a sinogram for vector field ($\boldsymbol{u}(\boldsymbol{r}')$) multiplied by $\epsilon_0(\boldsymbol{r}')$. After deriving the sinogram of 0^{th} and 1^{st} spectral moments, the $\epsilon_0(\boldsymbol{r}')$ and the $\boldsymbol{u}(\boldsymbol{r}')$ can be reconstructed. The reconstruction method of local velocity vector from sinograms was already discussed in the literature [9] and is summarized in Appendix A.

3. Feasibility Test

3.1 Numerical simulation

The method was evaluated using a numerical turbulence simulation for linear magnetized plasma, the Numerical Linear Device (NLD) code [14, 15]. The calculation conditions were similar to the typical parameters of linear magnetized plasma; Argon gas, 0.1 T magnetic field strength, 3 eV electron temperature, ~ 20 cm plasma diameter, electron-neutral collision frequency $\nu_{in}/\omega_{ci} = 0.035$ where ω_{ci} is the ion cyclotron frequency. Other parameters were described in Ref. [15]. Under these conditions, the resistive drift wave turbulence and the zonal flow were excited.

The results of the numerical simulation are shown in Fig. 2. Figure 2 (a) shows the spatio-temporal behavior of

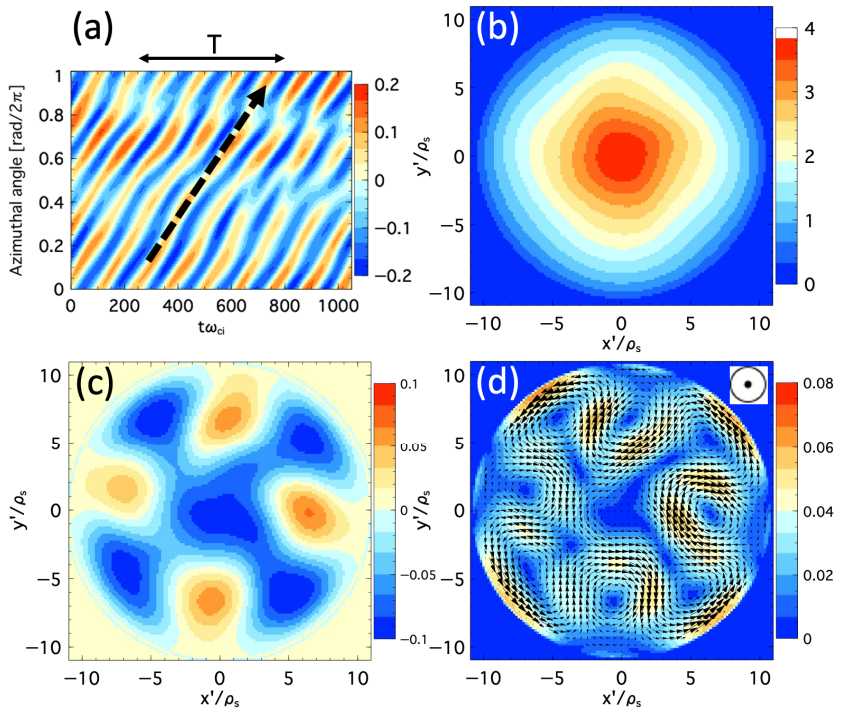

Fig. 2 Calculated results of the Numerical Linear Device (NLD) simulation. (a) Spatio-temporal structure at a radius of r/ρ_s=9.1. The two-dimensional structure of (b) plasma density (used as $\epsilon_0(\boldsymbol{r}')$) and (c) potential. (d) The velocity vector field of the ion (vector arrows), $\boldsymbol{u}(\boldsymbol{r}')$, and the velocity amplitude of the ion (filled contour), $|\boldsymbol{u}(\boldsymbol{r}')|$.

the density at a radius of $r/\rho_s = 9.1$, where the positive direction denotes the electron diamagnetic direction, ρ_s denotes the effective gyro radius and temporal evolution with the factor of ω_{ci}. As shown in Fig. 2 (a), the dotted arrow indicates the propagation direction of the azimuthal structure, which rotates quasi-periodically. Figures 2 (b) and (c) present the planar cross-sectional images of plasma density and potential averaged over a cycle along the propagation direction, where the potential was normalized as $e\psi/T_e$. The two-dimensional vector fields of Argon ion are shown in Fig. 2 (d), where filled contour indicates the amplitude of ion velocity, which is normalized by sound velocity (c_s). Here, we estimated that the flow is incompressible and divergence-free, dominated by the $E\times B$ drift.

Note that the electron temperature was set to be spatially uniform in the measurement simulations. Thus in the three-level LIF scheme for Argon ions in this study, the ion density distribution of the ground state was assumed to be proportional to the ion density distribution of the metastable state, which is related to the fluorescence intensity. It was also assumed that the plasma is optically thin and the optical system are well collimated. In other words, the simulated collection intensity was assumed to be proportional to the fluorescence intensity and, thus, to the ion density distribution of the ground state. Based on the above, for simplicity, the measurement simulations in this study were performed with the plasma density, or the ion density distribution of the ground state, as $\epsilon_0(\boldsymbol{r}')$.

3.2 Reconstruction of ideally-coherent structure

In this subsection, the results of the reconstruction procedure with using the ideally coherent structure are presented. The data shown in Figs. 2 (b) - (d) are used for the sinograms with rotating same angular velocity. The numerical results were down-sampled to a resolution close to that of the practical measurements to simulate the practical measurements. Since the LMD-U and PANTA devices have 64-channel azimuthal probe array, the resolution of the ϕ, $\Delta\phi$, was determined as $\Delta\phi = 2\pi/64$ rad [1]. The operational condition of laser sweep range was 10 GHz with 0.1 GHz spacing. To cover the plasma area, x is selected as 42 points, which is about 2.5 mm spacing in terms of practical measurement. The resulting sinograms of the spectral moments $\mu^{(0)}$ or $\mu^{(1)}$ are shown in Figs. 3 (a) or (b).

The sinograms were interpolated in x and ϕ directions before the reconstruction to avoid the conversion error between Cartesian and polar coordinates. Here, the direction of x or ϕ was up-converted from 42 points to 128 points or from 64 points to 512 points. The filtered-back-projection method with Ram-Lak filter and zero-padding (factors of 4 for x direction) was applied for the reconstruction process [19].

Figure 4 (a) presents the reconstructed $\epsilon_0(\boldsymbol{r}')$, while Fig. 4 (b) illustrates the reconstructed $\boldsymbol{u}(\boldsymbol{r}')$. Figure 4 (c) presents the amplitude of $\boldsymbol{u}(\boldsymbol{r}')$. The comparison of Fig. 4 (b) and Fig. 2 (d) shows that the flow patterns are similar around the central region but not at the edge region.

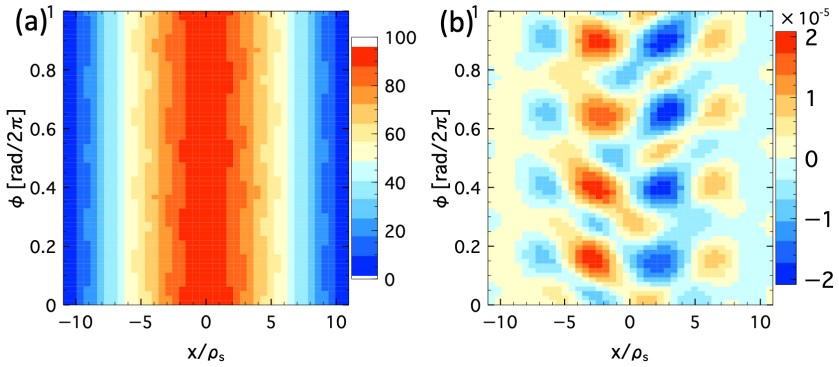

Fig. 3 Sinogram of the spectral moment on (a) the 0^{th} order moment ($\mu^{(0)}$) and (b) the 1^{st} order moment ($\mu^{(1)}$).

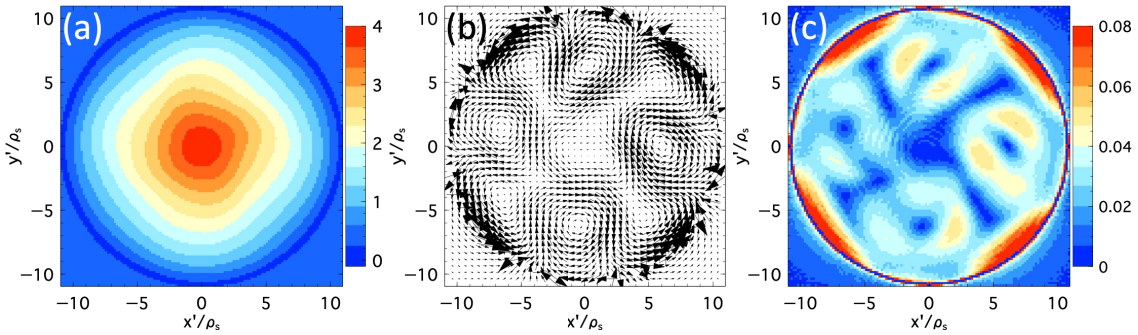

Fig. 4 Reconstructed image of (a) $\epsilon_0(\boldsymbol{r}')$, (b) $\boldsymbol{u}(\boldsymbol{r}')$ and (c) amplitude of $\boldsymbol{u}(\boldsymbol{r}')$. For simplicity, the light collection efficiency was set to be 1.

In addition, the values at the edge region are much higher than that of the ideal case. This discrepancy in values is because the reconstruction of velocity field requires normalization with fluorescence intensity (see Appendix A). Moreover, the discrete noise, gridding, filtering, interpolating and coordinate transformation are enlarged at the edge region.

Our method can evaluate the azimuthal Reynolds stress and Reynolds force as the axial symmetry of the plasma is not assumed. The evaluated Reynolds stress, $< \pi_{r\theta} >$, is shown as points in Fig. 5 (a), where the values were down-sampled to the original (42 points) (see Appendix B). The dashed line was obtained directly by the result of the turbulence simulation (Fig. 2 (d)). The Reynolds force was also evaluated as $-\partial_r < r\pi_{r\theta} > /r$. Here, the $< r\pi_{r\theta} >$ was smoothed before differentiating as the radial derivative to enhance the noise in the case of discrete measurement. The result is shown by points in Fig. 5 (b). Here, the dashed line was also obtained by the result of turbulence simulation. The evaluated Reynolds stress and Reynolds force are consistent with the ideal values, except at the edge. The difference in values observed at the edge is caused by the reconstruction error of the density similar to those in Fig. 4 (b). Moreover, slight differences were observed in the peaks and radial position probably due to the down-sampling of the measurement points.

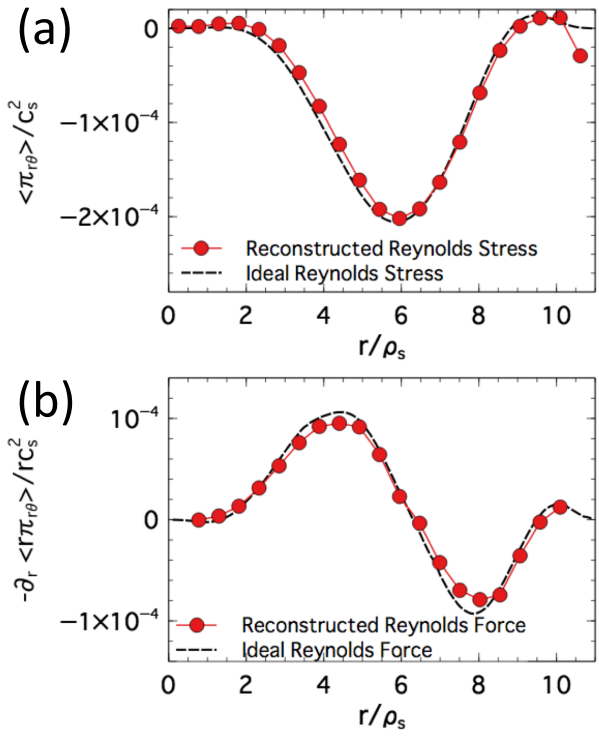

Fig. 5 Radial profile of (a) Reynolds stress and (b) Reynolds force. The dashed-lines are the ideal values calculated by the numerical turbulence simulation (Fig. 1 (d)).

3.3 Reconstruction of quasi-coherent structure

Here, we directly used the result of numerical simulation. Although the plasma was rotating periodically, the propagation angular velocity of the structure at each radial position was not the same. Figure 6 (a) shows the relative angular velocity of the structure normalized by the value at $r/\rho_s = 9.1$. The angular velocity around the center of plasma was faster than that of the edge region. The reconstruction procedure was similar to the described in previous subsection 3.2, but the ~ 5 cycles of data with referring the phases at $r/\rho_s = 9.1$ were used. Reconstructed Reynolds stress and Reynolds force and their corresponding ideal values obtained directly from numerical simulation results are shown in Figs. 6 (b) and (c). As shown in the figures, the reconstructed values of Reynolds stresses and Reynolds forces are similar to the corresponding ideal values at the outer region, except at the edge. The evaluated Reynolds stress and Reynolds force are consistent with ideal values (less than 20%, $r/\rho_s > 5$) at the case when the difference of propagation angular velocity is less than 20% compared with the values at the reference. However, around the central region, the evaluated Reynolds stress and Reynolds force are much lower than the corresponding ideal values. This is because our method assumes that the propagation of the flow structure is rotating with constant angular velocity; the velocity difference with the reference position causes underestimation of the reconstructed velocity.

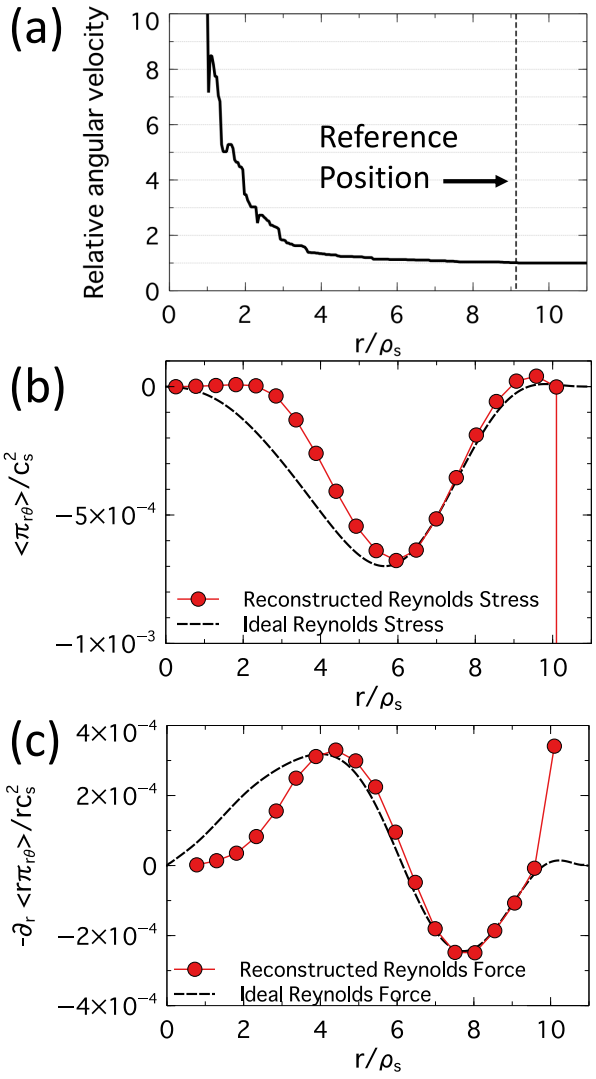

Fig. 6 (a) Radial profile of propagation angular velocity relative to the velocity at $r/\rho_s = 9.1$. The radial profile of (b) Reynolds stress and (c) Reynolds force. The lines are the ideal values calculated.

4. Discussion

The measurement time requirements of this measurement conditions are discussed here: from 64-channel Langmuir probe measurements, 100 laser frequency changes and 42 laser incidence position conditions, it is estimated that a total of 268,800 fluorescence intensity conditions need to be detected for two-dimensional flow vector reconstruction. Both the LMD-U and the PANTA devices discharge for 0.5 s and the plasma fluctuation characteristics are steady 0.2 s after the start of discharge [20], thus a measurement time of 0.3 s per discharge is expected to be obtained. In addition, these devices observed drift wave type modes at a frequency of several kHz [3, 5]. Then, if the flow pattern is assumed to take 1 ms per cycle, it can be measured during 300 rotations during a discharge. Scanning the laser frequency during plasma discharge is also expected to be an effective measurement, as in [20]. Also, the laser intensity is modulated by electro-optical modulator to eliminate the background emissions, which is $\sim$ 200 kHz in the PANTA system [20], well faster than the targeted flow pattern rotation and laser frequency shift. Thus, ideally, in a single discharge, it is possible to measure the fluorescence intensity under the defined conditions of ϕ and ν at a certain laser incidence position x. Considering that the laser incidence position is changed for each discharge, the fluorescence intensity can be measured under 268,800 conditions in 42 discharges. However, because of the influence of noise, ensemble averaging is required by repeated measurements. For example, if measurements for 10 discharges (300 rotations/discharge $\times$ 10 discharge = 30,00 plasma rotations) are assumed, the measurement time is about 2 hours with discharge repetitions at 10 second intervals. The required number of repetitive discharges depends on the noise conditions and should be a subject for future work.

A limitation of our method is that it assumes that the flow structure rotates without change. The difference in propagation angular velocity causes underestimation of the velocity field. Nevertheless, if the propagation velocity at each radial location is known, reconstruction errors can be corrected and the accuracy of the velocity field can be improved. The time delay estimation method [21] can be used

to measure the propagation velocity by using radially movable Langmuir probes, which has multiple (≥2) probes in the azimuthal direction. Each radial value is recovered by replacing the phase of the sinogram as $\alpha\phi$, where the α denotes the coefficient of each angular velocity by referring the value at the probe array.

5. Summary

In this study, we proposed a vector tomography method for reconstructing a two-dimensional velocity field of quasi-coherent structure in linear magnetized plasma. For this, the azimuthal reference probe array and laser injection with single-injection angle were synchronized to reconstruct the multi-projection angle of line-integrated LIF. The proposed method assumed that the flow structure propagated periodically in the azimuthal direction without change. The method was applied to the flow structure obtained by direct numerical simulation. Two-dimensional ion velocity field was reconstructed by evaluating the spectral moments considering the practical measurement resolution. The radial profile of Reynolds stress and Reynolds force were consistent with the corresponding ideal values where the propagation angular velocity of the flow structure was close to the velocity at the reference probe array.

Acknowledgments

This work has been supported by the grant-in-aid for Scientific Research of JSPS KAKENHI (Grant Numbers JP17H06089, JP15H02335, JP21K03508 and JP21K03509), by the Collaborative Research Programme of Research Institute for Applied Mechanics, Kyushu University and by the Shimadzu Science Foundation.

Appendix A. Flow Field Reconstruction Procedure

The calculation process for the reconstruction of two-dimensional velocity field is discussed in the following steps. The spectral integration of fluorescence, $\epsilon_0(\boldsymbol{r}')$, should be reconstructed before the calculation of the $\boldsymbol{u}(\boldsymbol{r}')$. The $\epsilon_0(\boldsymbol{r}')$ can be reconstructed with conventional tomographic method, *e.g.*, filtered-back-projection [19]. The vector field $\epsilon_0(\boldsymbol{r}')\boldsymbol{u}(\boldsymbol{r}')$ can be reconstructed in each direction separately (x'- or y'-direction) as [18],

$$\{\epsilon_0(\boldsymbol{r}')\boldsymbol{u}(\boldsymbol{r}')\}_{x'} = \mathcal{F}_{2\mathrm{D}}^{-1}[\sin(-\phi)\mathcal{F}[\mu^{(1)}]], \quad (A.1)$$

$$\{\epsilon_0(\boldsymbol{r}')\boldsymbol{u}(\boldsymbol{r}')\}_{y'} = \mathcal{F}_{2\mathrm{D}}^{-1}[-\cos(-\phi)\mathcal{F}[\mu^{(1)}]], \quad (A.2)$$

where the $\mathcal{F}$ denotes the one-dimensional Fourier transform relative to x, $\mathcal{F}[\mu^{(1)}](k,\phi) = \int_{-\infty}^{\infty}\mu^{(1)}\exp(-ikx)dx$, and $\mathcal{F}_{2\mathrm{D}}^{-1}$ denotes the two-dimensional inverse Fourier transform. Here, this reconstruction method is applicable in the case of divergence-free flow [18]. A conventional tomographic reconstruction method can be applied to the calculation of $\mathcal{F}_{2\mathrm{D}}^{-1}$ in Eqs. (A.1) and (A.2), such as the filtered-back-projection. The two-dimensional velocity field can be recovered as $\boldsymbol{u}(\boldsymbol{r}') = (u_{x'}(\boldsymbol{r}'), u_{y'}(\boldsymbol{r}')) = (\{\epsilon_0(\boldsymbol{r}')\boldsymbol{u}(\boldsymbol{r}')\}_{x'}/\epsilon_0(\boldsymbol{r}'), \{\epsilon_0(\boldsymbol{r}')\boldsymbol{u}(\boldsymbol{r}')\}_{y'}/\epsilon_0(\boldsymbol{r}'))$. Note that, the cross-section image on ion temperature can also be reconstructed with 2^{nd} order spectral moment [9].

Appendix B. Evaluation of Reynolds Stress

The velocity field from Cartesian to Polar coordinates was converted to evaluate the radial Reynolds stress and Reynolds force as,

$$u_{r'}(\boldsymbol{r}') = \frac{\{\epsilon_0(\boldsymbol{r}')\boldsymbol{u}(\boldsymbol{r}')\}_{x'}\cos\theta' + \{\epsilon_0(\boldsymbol{r}')\boldsymbol{u}(\boldsymbol{r}')\}_{y'}\sin\theta'}{\epsilon_0(\boldsymbol{r}')}, \quad (B.1)$$

$$u_{\theta'}(\boldsymbol{r}') = \frac{-\{\epsilon_0(\boldsymbol{r}')\boldsymbol{u}(\boldsymbol{r}')\}_{x'}\sin\theta' + \{\epsilon_0(\boldsymbol{r}')\boldsymbol{u}(\boldsymbol{r}')\}_{y'}\cos\theta'}{\epsilon_0(\boldsymbol{r}')}, \quad (B.2)$$

where $\theta' = \arctan(y'/x')$, $u'_r(\boldsymbol{r}')$ denotes the radial component of the velocity field, and $u_{\theta'}(\boldsymbol{r}')$ denotes the azimuthal component of the velocity field. The Reynolds stress at each radial position is the same in the stationary and rotating coordinate systems and can be shown as,

$$< \pi_{r\theta} > = < \tilde{v}_r\tilde{v}_\theta > = < \tilde{v}_{r'}\tilde{v}_{\theta'} > = < \tilde{u_{r'}}\tilde{u_{\theta'}} > c^2, \quad (B.3)$$

where the ˜ indicates the fluctuation component at each radius, and <> indicates the ensemble averaging through the azimuthal direction.

[1] T. Yamada, S.-I. Itoh, T. Maruta, N. Kasuya, Y. Nagashima, S. Shinohara, K. Terasaka, M. Yagi, S. Inagaki, Y. Kawai *et al.*, Anatomy of plasma turbulence. Nature Phys. **4(9)**, 721 (2008).

[2] H. Arakawa, S. Inagaki, M. Sasaki, Y. Kosuga, T. Kobayashi, N. Kasuya, Y. Nagashima, T. Yamada, M. Lesur, A. Fujisawa *et al.*, Eddy, drift wave and zonal flow dynamics in a linear magnetized plasma. Sci. Rep. **6**, 33371 (2016).

[3] H. Arakawa, M. Sasaki, S. Inagaki, Y. Kosuga, T. Kobayashi, N. Kasuya, T. Yamada, Y. Nagashima, F. Kin, A. Fujisawa *et al.*, Roles of solitary eddy and splash in drift wave–zonal flow system in a linear magnetized plasma. Phys. Plasmas **26(5)**, 052305 (2019).

[4] P.H. Diamond, S.-I. Itoh, K. Itoh and T.S. Hahm, Zonal flows in plasma—a review. Plasma Phys. Control. Fusion **47(5)**, R35 (2005).

[5] H. Arakawa, S. Inagaki, Y. Nagashima, T. Yamada, K. Kamataki, T. Kobayashi, S. Sugita, M. Yagi, N. Kasuya, A. Fujisawa *et al.*, Bifurcation of the plasma turbulence on lmd-u. Plasma Phys. Control. Fusion **52(10)**, 105009 (2010).

[6] H. Arakawa, K. Kamataki, S. Inagaki, T. Maruta, Y. Nagashima, T. Yamada, S. Shinohara, K. Terasaka, S. Sugita, M. Yagi *et al.*, Observations of abrupt changes in the fluctuation spectrum on lmd-u. Plasma Phys. Control. Fusion **51(8)**, 085001 (2009).

[7] S. Inagaki, T. Kobayashi, Y. Kosuga, S.-I. Itoh, T. Mitsuzono, Y. Nagashima, H. Arakawa, T. Yamada, Y. Miwa, N. Kasuya *et al.*, A concept of cross-ferroic plasma turbulence. Sci. Rep. **6**, 22189 (2016).

[8] A. Fujisawa, Y. Nagashima, S. Inagaki, T. Onchi, S. Ohshima and A. Shimizu, Tomography as a promising diagnostic tool for plasma turbulence. Plasma Phys. Control. Fusion **58(2)**, 025005 (2016).

[9] J. Howard, Vector tomography applications in plasma diagnostics. Plasma Phys. Control. Fusion **38(4)**, 489 (1996).

[10] R. Lester, Y. Zhai, C. Corr and J. Howard, Coherence imaging for ion temperature and flow measurements in a low-temperature helicon plasma source. Plasma Sources Sci. Technol. **25(1)**, 015025 (2016).

[11] A.L. Balandin, Y. Murata and Y. Ono, Radial velocity profile reconstruction by doppler spectroscopy measurements. The European Physical Journal D-Atomic, Molecular, Optical Plasma Phys. **27(2)**, 125 (2003).

[12] A.L. Balandin and Y. Ono, Tomographic determination of plasma velocity with the use of ion doppler spectroscopy. The European Physical Journal D-Atomic, Molecular, Optical Plasma Phys. **17(3)**, 337 (2001).

[13] Y. Kawaguchi, N. Kobayashi, Y. Yamagata, F. Miyazaki, M. Yamasaki and K. Muraoka, Spatially-resolved velocities of thermally-produced spray droplets using a velocity-divided abel inversion of photographed streaks. J. Physics D: Appl. Phys. **50(42)**, 425203 (2017).

[14] N. Kasuya, M. Yagi, M. Azumi, K. Itoh and S.-I. Itoh, Numerical simulation of resistive drift wave turbulence in a linear device. J. Phys. Soc. Jpn. **76(4)**, 044501 (2007).

[15] M. Sasaki, N. Kasuya, K. Itoh, S. Toda, T. Yamada, Y. Kosuga, Y. Nagashima, T. Kobayashi, H. Arakawa, K. Yamasaki *et al*., Topological bifurcation of helical flows in magnetized plasmas with density gradient and parallel flow shear. Phys. Plasmas **24(11)**, 112103 (2017).

[16] R.A. Stern and J.A. Johnson, Plasma ion diagnostics using resonant fluorescence. Phys. Rev. Lett. **34(25)**, 1548 (1975).

[17] F. Anderegg, R.A. Stern, F. Skiff, B.A. Hammel, M.Q. Tran, P.J. Paris and P. Kohler, Ion heating due to rotation and collision in magnetized plasma. Phys. Rev. Lett. **57(3)**, 329 (1986).

[18] S.J. Norton, Tomographic reconstruction of 2-d vector fields: application to flow imaging. Geophys. J. Int. **97(1)**, 161 (1989).

[19] J. Hseih, *Computed Tomography - Principles, Design, Artifacts and Recent Advances*, 01 (2009).

[20] H. Arakawa, S. Inagaki, Y. Kosuga, M. Sasaki, F. Kin, K. Hasamada, K. Yamasaki, T. Kobayashi, T. Yamada, Y. Nagashima *et al*., Ion temperature measurement by laser-induced fluorescence spectroscopy in panta. IEEJ Trans. Electr. Electron. Eng. **14(10)**, 1450 (2019).

[21] Y. Nagashima, S.-I. Itoh, S. Shinohara, M. Fukao, A. Fujisawa, K. Terasaka, Y. Kawai, N. Kasuya, G.R. Tynan, P.H. Diamond *et al*., Coexistence of zonal flows and drift-waves in a cylindrical magnetized plasma. J. Phys. Soc. Jpn. **77(11)**, 114501 (2008).